JACS
JOURNAL OF THE AMERICAN CHEMICAL SOCIETY
Article
pubs.acs.org/JACS

Size and Structure Matter: Enhanced CO_2 Photoreduction Efficiency by Size-Resolved Ultrafine Pt Nanoparticles on TiO_2 Single Crystals

Wei-Ning Wang,[†,#] Woo-Jin An,[†,#] Balavinayagam Ramalingam,[‡] Somik Mukherjee,[‡] Dariusz M. Niedzwiedzki,[§] Shubhra Gangopadhyay,[‡] and Pratim Biswas*[,†]

[†]Aerosol and Air Quality Research Laboratory, Department of Energy, Environmental, and Chemical Engineering and
[§]Photosynthetic Antenna Research Center, Washington University in St. Louis, St. Louis, Missouri 63130, United States
[‡]Center for Micro/Nano Systems & Nanotechnology, University of Missouri, Columbia, Missouri 65211, United States

Supporting Information

ABSTRACT: A facile development of highly efficient Pt-TiO_2 nanostructured films via versatile gas-phase deposition methods is described. The films have a unique one-dimensional (1D) structure of TiO_2 single crystals coated with ultrafine Pt nanoparticles (NPs, 0.5−2 nm) and exhibit extremely high CO_2 photoreduction efficiency with selective formation of methane (the maximum CH_4 yield of 1361 μmol/g-cat/h). The fast electron-transfer rate in TiO_2 single crystals and the efficient electron−hole separation by the Pt NPs were the main reasons attributable for the enhancement, where the size of the Pt NPs and the unique 1D structure of TiO_2 single crystals played an important role.

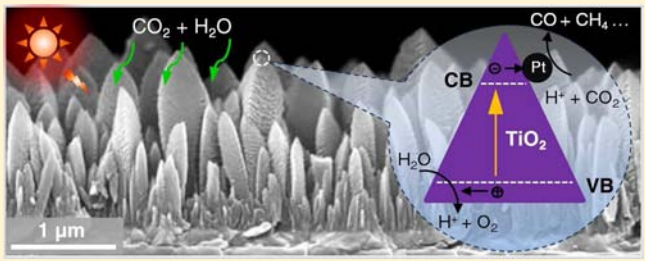

INTRODUCTION

Increasing anthropological emissions of greenhouse gases, in particular carbon dioxide (CO_2) into the atmosphere is widely recognized to be one of the primary causes of global climate change. In addition to carbon capture and sequestration (CCS) technology,[1] a desirable strategy is to convert CO_2 by reduction to a fuel or other useful chemicals. To this end, we face an energy intensive challenge in its reduction since CO_2 is very stable.[2−4] Developing an efficient photocatalyst appears to be a promising methodology to meet this challenge, and this has been a prominent quest to convert CO_2 into hydrocarbon fuels.[2−5] Various photocatalysts have been developed including semiconductors, such as TiO_2, ZnO, CdS, and $ALa_4Ti_4O_{15}$ (A = Ca, Sr, and Ba) and organic compounds, e.g., rhenium complexes.[5] The photocatalysis process can be sustainable by harnessing solar energy, making it economically feasible and environmentally benign. In spite of the above-mentioned advantages, CO_2 photoreduction, however, still suffers from very low conversion efficiencies, resulting from the fast electron−hole recombination rate in the photocatalysts; a major barrier that needs to be overcome.

Several strategies have been proposed to solve this problem, such as use of mesoporous structures and metal doping.[2,3] The synergistic effect of both strategies has also been investigated.[6,7] Among them, surface platinization has been a popular technique since its first introduction by Kraeutler and Bard.[8] The platinum (Pt) nanoparticles (NPs) are believed to retard electron−hole recombination by serving as electron sinks and to facilitate interfacial electron transfer.[9,10] These Pt NPs were primarily prepared by wet chemical methods, in which the particle size and size distribution were not easily controlled.[11] In addition to trapping electrons, large Pt NPs may also consume holes, thus serving as recombination centers.[12] Contamination is another drawback since the Pt NPs prepared by liquid methods are easily oxidized owing to chemical residues on surfaces, resulting in deteriorated performance.[13] Moreover, the catalysts developed thus far are mostly powders, in which the grain boundary effect cannot be avoided.[9] Hence the reported highest yield of carbon monoxide (CO), a major product of CO_2 photoreduction, has been limited to less than 200 μmol/g-cat/h.[2,14]

Here we report a facile development of highly efficient platinized titanium dioxide (Pt-TiO_2) nanostructured films via versatile gas-phase deposition methods.[15,16] The TiO_2 films were deposited using an aerosol chemical vapor deposition (ACVD) route,[15,17] which is a continuous and low-energy method designed to deposit metal oxide films with controlled morphologies. The columnar TiO_2 films were selected in this work for Pt deposition owing to their high surface area, single crystallinity, and superior electron-transfer performance originating from highly oriented one-dimensional (1D) structures.[15,17] Platinum NPs were deposited onto the TiO_2 single crystals using a unique tilted-target sputtering (TTS) method.[16] The TTS configuration allows one to control the flux of sputtered metal atoms and their radial distribution. The low energy of the arriving metal atoms outside the focal area of deposition reduces the surface Brownian motion on the substrate and slows down the coalescence, which helps formation of ultrafine Pt NPs with narrow size distribution.

Received: April 27, 2012
Published: June 14, 2012

Table 1. Characterization of Pt-TiO_2 Thin Films

samples	average Pt particle size[a] (nm)	Pt number density ($\times 10^{12}$/cm^2)[a]	Pt atomic percentage[b] (%)	Pt oxidation states (before/after)[b]	O/Ti atomic ratio[b]	CH_4 yield (μmol/g-cat/h)[c]
Pt_5s	<0.5	<2	NA	NA	NA	292
Pt_10s	0.63 ± 0.06	4.81	0.21	$Pt^0/Pt^0,Pt^{II}$	2.31/2.60	415
Pt_15s	0.82 ± 0.09	5.02	NA	NA	NA	557
Pt_20s	1.04 ± 0.08	5.20	0.94	Pt^0/Pt^0	2.29/2.50	1361
Pt_25s	1.22 ± 0.12	4.97	NA	NA	NA	746
Pt_30s	1.34 ± 0.15	5.35	1.34	Pt^0/Pt^0	2.30/2.51	631
Pt_45s	1.61 ± 0.22	4.92	NA	NA	NA	424
Pt_60s	1.87 ± 0.31	5.12	2.49	Pt^0/Pt^0	2.35/2.47	63

[a]Measured from TEM images (see Figures S8 and S9, Supporting Information for examples). [b]Analyzed by XPS (see Figure S7, Supporting Information for details). [c]Obtained from photoreduction analysis.

■ EXPERIMENTAL SECTION

Thin Film Deposition by ACVD. The experimental conditions for the ACVD system to deposit TiO_2 thin films with different morphologies have been explained previously[15,17] and are briefly described here (see Supporting Information, S1, for more details). Titanium tetraisopropoxide (TTIP, 97%, Sigma-Aldrich) was used as a precursor and loaded in a homemade bubbler at a constant temperature of 297 K. The deposition substrate was indium tin oxide (ITO)-coated aluminumosilicate glass (Delta Technologies) which was maintained at 773 K for all samples. The flow rate of carrier gas, nitrogen (N_2), entering the bubbler was controlled at 0.47 L per minute (lpm), which was equivalent to 1.53 μmol/min of TTIP fed into the reactor. The total flow rate including dilution flow was 0.9 lpm, which corresponded to 20 ms of the residence time of TTIP. For all samples, the total deposition time of TiO_2 was fixed at 50 min. The mass of each thin film sample was theoretically estimated to be around 0.7 mg, which was confirmed by measurement.

Surface Platinization by TTS. The as-prepared TiO_2 thin films were transferred to an ATC 2000 V sputtering system (AJA International, Inc.). Platinum NPs were deposited using a TTS configuration with a target angle of 23.8°, 6 in. target−substrate distance, 4 mTorr operating pressure, and a fixed deposition power of 30 W with a varying deposition time. The TiO_2 thin film samples were placed in the outer region of the deposition flux zone where low-energy atoms took part in nanoparticle formation, thereby forming uniform ultrafine particles. The direct deposition method produces Pt NPs with diameters ranging from 0.5 to 2 nm for deposition times of 5−60 s (see Supporting Information, S1). The average particle size and particle number density were measured from the corresponding TEM images and summarized in Table 1.

Thin Film Characterization. The morphology of the thin films was examined using field emission scanning electron microscopy (FE-SEM) (NOVA NanoSEM 230, FEI Co.) operated at 15 kV. Average film height and column (single crystal) diameter were estimated from the FE-SEM images. The morphology of the films was also evaluated by atomic force microscopy (AFM) (Dimension 3100 Nanoman, Veeco Instruments, Inc.). Elemental mapping of the films was characterized by energy dispersive X-ray spectroscopy (EDX). The inner structure of the films was analyzed by transmission electron microscopy (TEM) (JEM-2100F, JEOL). The crystal phase was determined by X-ray diffraction (XRD) (Geigerflex D-MAX/A, Rigaku Denki) using CuK_α radiation (λ = 1.548 Å). The optical properties of the thin films were measured by ultraviolet−visible (UV−vis) absorption spectroscopy (Cary 100, Varian Inc.) at room temperature. The Pt oxidation states before and after photoreduction were analyzed by X-ray photoelectron spectroscopy (XPS) (AXIS 165, Kratos Analytical) with monochromated aluminum as an anode operated at 150 W.

Femtosecond Time-Resolved Transient Absorption (TA) Spectroscopy Measurements. The measurements were carried out using a femtosecond TA spectrometer (Helios, Ultrafast Systems) coupled to a femtosecond laser system consisting Solstice (Spectra-Physics) built of a Ti:sapphire regenerative amplifier (Spitfire Pro XP), a pulse stretcher and compressor, a femtosecond oscillator (Mai-Tai) as seeding source, and a diode-pumped solid-state pulsed green laser (Empower) as the pump source. The system produced pulses centered at 800 nm with energy of ∼3.5 mJ, ∼90 fs duration, and 1 kHz repetition rate. Ninety percent of the output beam was used to generate pump beam in an optical parametric amplifier (Topas-C with Berek extension) (Light Conversion Ltd.). The remaining 10% was used to produce probe pulses in the Helios spectrometer. A near-infrared continuum probe was generated by a proprietary crystalloid plate. A 256 pixel InGaAs linear diode array was used as a detector. To provide an isotropic excitation of the sample and avoid pump−probe polarization effects, the pump beam was depolarized using depolarizer. The samples were excited at 365 nm with pump beam energy kept at low energies between 1 and 3 μJ. The excitation beam was focused to a spot size of 1 mm diameter corresponding to photon intensity of 2.34−7.04 $\times 10^{14}$ photons/cm^2. Detailed data analysis can be found in Supporting Information, S11.

Photoreduction Analysis. The photoreduction analysis system is described in a previous paper.[7] Compressed CO_2 was used as the carbon source. It passed through a water bubbler to generate a mixture of CO_2 and water vapor. The gaseous mixture was then fed into a continuous flow reactor where the films were loaded. The reactor is cylindrical in shape with a quartz window vertically facing the light source, which is a Xe lamp operated at 400 W with an accumulated intensity of 19.6 mW/cm^2 in the effective UV range (250−388 nm) (see Supporting Information, S4). Before each test, the reactor loaded with samples was first purged with CO_2 and water vapor at 100 mL/min for 1 h, and then the flow rate was reduced and maintained at 3 mL/min during the whole analysis process. The concentrations of effluent gases as a function of irradiation time were recorded automatically by gas chromatography (GC) through an automated gas valve, using helium as the carrier gas. The GC was equipped with a PLOT capillary column (Supelco Carboxen-1010) and a thermal conductivity detector.

■ RESULTS AND DISCUSSION

A representative Pt-TiO_2 thin film was characterized by FE-SEM, AFM, elemental mapping, TEM, XRD, and UV−vis (Figure 1). As shown in Figure 1a, the Pt-TiO_2 film has a highly oriented 1D structure with a typical column diameter of 250 nm, which significantly increases the effective surface area compared to a planar film, providing more active sites for photocatalytic reactions (see Supporting Information, S2 for an estimation of surface area of the columnar films). The highly oriented morphology of the film was also confirmed by AFM (Figure 1b), where the height was estimated to be around 1.5 μm. Corresponding elemental mapping (Figure 1c) and TEM analysis (Figure 1d) confirm the presence of Pt NPs on the surface of TiO_2 single crystals. The high-resolution (HR)-TEM analysis reveals that the single crystals have an orientation of anatase (112) plane, and surface defects are also observed (Figure 1d inset). These defects or dislocations are the reason

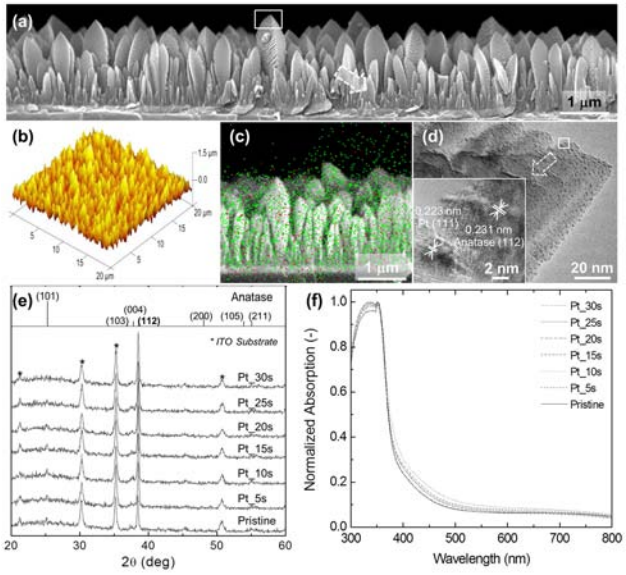

Figure 1. Characterization of a representative columnar TiO_2 thin film loaded with Pt NPs for a deposition time of 20 s at 30 W. (a) FE-SEM image of the thin film, where the white rectangle indicates the location of TEM image. (b) AFM image (3D view). (c) Composed elemental mapping image, where green denotes Ti and red indicates Pt. (d) TEM images, where the square indicates the location of HR-TEM image. (e) XRD patterns, where the stars designate the background of the ITO substrate, and (f) UV−vis absorption spectra of pristine TiO_2 and Pt-TiO_2 samples with different Pt deposition times.

for oriented attachment of particles/molecules to form (112) orientation[18] and the active sites for Pt deposition.[16] The high surface energy of the (112) plane is preferred since it can enhance the electron mobility and hence improve photocatalytic activity.[18,19] As seen in Figure 1d, the Pt NPs are partially crystallized and have an average diameter of 1 nm. It should be noted that these are extremely small Pt NPs achievable only by gas-phase deposition using our unique sputtering method. The 1D structure of the TiO_2 single crystals was also analyzed by XRD (Figure 1e), where a prominent (112) peak was observed. The corresponding Lotgering's factor[20] was calculated to be 0.52, indicating high orientation of the (112) plane. The optical properties of the films (Figure 1f) are not influenced by Pt coating since the difference of absorbance between pristine TiO_2 and Pt-TiO_2 films in 200−300 nm (absorption region of Pt NPs) is not significant (see Supporting Information, S3, for details).

The Pt-TiO_2 thin films were then subjected to CO_2 photoreduction analysis. Representative CO and methane (CH_4) yields of the film versus irradiation time were plotted (Figure 2a). The film demonstrated high selectivity to CH_4 formation. The CH_4 yield increased with irradiation time and reached a peak value of 1361 μmol/g-cat/h at 5 h. The quantum yield at this condition was calculated to be 2.41% (see Supporting Information, S4, for calculation). To the best of our knowledge, this value is the highest CH_4 yield ever reported in the literature of photoreduction of CO_2.[2−5,14,21] Hydrogen (H_2) could not be detected indicating that the amount evolved in this work was not significant and probably all reacted. It is also worth noting that the actual overall quantum yield of CO_2 photoreduction of the Pt-TiO_2 thin films could be even higher since only products with low molecular weights (MWs), such as CO and CH_4 signals, could be detected by the GC column that

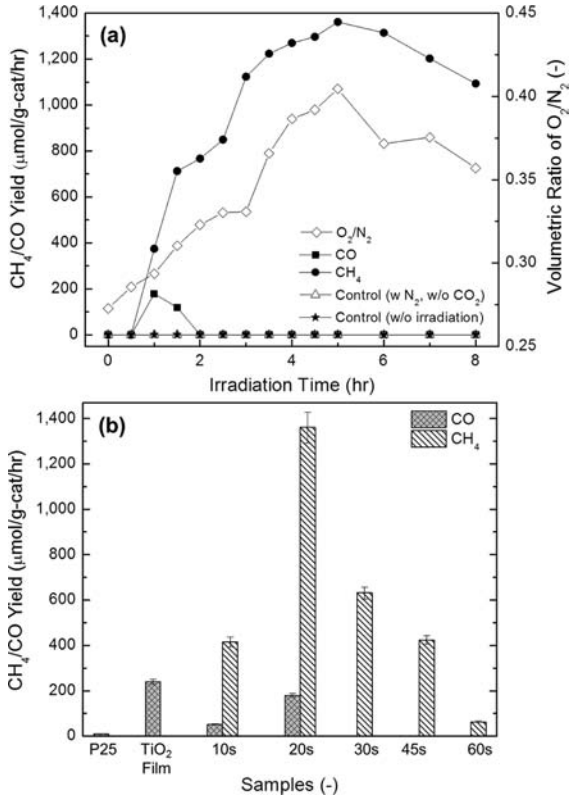

Figure 2. Photoreduction analysis of Pt-TiO_2 thin films. (a) Representative CH_4 and CO yields on a Pt-TiO_2 thin film (Pt deposition time of 20 s) as a function of irradiation time (solid circles and squares, ● and ■, respectively). Open triangles, △, indicate control experiments with illumination but without CO_2, and solid stars, ★, represent control experiments with flowing CO_2 but without illumination. The volumetric ratio of O_2/N_2 was also recorded (open diamonds, ◇). (b) CO and CH_4 yields of commercially available TiO_2 powders (P25), pristine TiO_2 columnar films (TiO_2 film), and Pt-TiO_2 films with different Pt deposition times.

was used in this study. Signals of some other potential products with larger MWs, such as HCO_2H, CH_2O, and CH_3OH, may be neglected as they are not probable to be formed. After 5 h of irradiation, CH_4 production rates started to drop slightly which can be attributed to deterioration of photocatalytic activity due to diminishment of the adsorption power of the catalyst[9] and the saturation of adsorption sites on the TiO_2 surface with intermediate products.[6,22] Carbon monoxide formation was also observed but with a lower yield, and it ceased after 2.5 h of irradiation due to the selective formation of CH_4 based on a six-electron reaction (see Supporting Information, SE6).[21] It should also be noted the synthesis methodology of the nanostructures allows the rapid desorption of products, a desirable feature in such systems.[23]

To better understand the mechanistic pathway of CH_4 formation, two control experiments were performed (Figure 2a). These are especially important to rule out possibilities of contamination from other carbon sources, for example, from incomplete oxidation of TTIP during fabrication of the TiO_2 films or oil contamination from vacuum pumps during Pt decoration. First, the films were illuminated without introducing CO_2 as the carbon source, where N_2 was used as the carrier gas. If there was any reactive residual carbon, it would react with protons (H^+) or H_2 generated based on competitive water splitting and form CH_4. Neither CH_4 nor other carbon

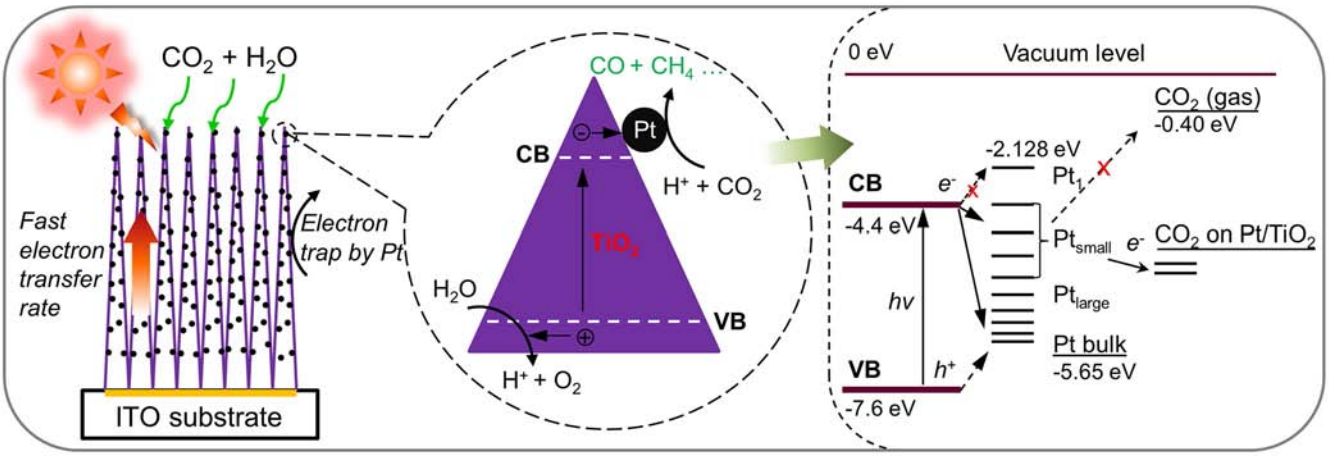

Figure 3. Schematic diagram of CO_2 photoreduction mechanism by using Pt-TiO_2 nanostructured films. The magnified circle (center) shows that the photogenerated electrons can move fast inside the highly oriented TiO_2 single crystals and flow to the Pt deposits, where the redox reaction occurs to convert CO_2 into CO and CH_4. The right side of the figure illustrates the energy levels of the Pt-TiO_2−CO_2 system. CB and VB are abbreviations of conduction band and valence band, respectively. H^+ and h^+ indicate proton and hole, respectively.

compounds were observed indicating that there was no residual carbon or other carbon contamination in the system. Another experiment was done by introducing CO_2 but without irradiation. Neither CH_4 nor CO was formed implying that TiO_2 is the only active catalyst. Volumetric ratio of O_2/N_2, which is another important indicator for proton generation, as a function of irradiation time also shows a very similar tendency as that of CH_4 formation (see Figure 2a). The highest O_2/N_2 ratio was above 0.40 (higher than that of air, viz. 0.26), implying adequate supply of protons (see Supporting Information, SE3).

Since the Pt NPs trap electrons very effectively, the effect of Pt deposition was investigated in detail. Figure 2b illustrates the CO and CH_4 yields of Pt-TiO_2 films with different Pt deposition times. The comparison between the Pt-TiO_2 films with commercial TiO_2 powders (Degussa P25) and pristine TiO_2 films has also been made. Both pristine and Pt-TiO_2 films out-perform P25 powders. Pt-TiO_2 films demonstrated even superior performance, where the CH_4 yields in most cases were well above 400 μmol/g-cat/h. The yield showed a sharp rise with a peak at a Pt deposition of 20 s. The relatively low CH_4 yield of the films with low Pt depositions is due to insufficient sites present to trap electrons. The XPS analysis also indicated that the Pt NPs under these conditions were partially oxidized to form Pt^{II} (see Table 1 and Supporting Information, S5), serving as recombination centers.[13] Beyond the optimal condition (>20 s deposition time), the Pt-TiO_2 films also demonstrated lower CH_4 yields. It is commonly known that with increasing Pt depositions the active surface sites of TiO_2 were blocked and hence resulted in lower performance. By careful TEM examination on the Pt-TiO_2 films, we found that it should not be the only reason since even for Pt deposition for 60 s, there are still plenty of surface sites on TiO_2 films (see Supporting Information, S6). Detailed photoreduction results are also summarized in Table 1.

To elucidate the understanding of this trend, the particle size analysis was performed based on the TEM observations. The results show that the Pt size increased with deposition time, from <0.5 nm at 5 s to ∼1.87 nm at 60 s of deposition times (see Table 1 and Supporting Information, S7). At very short deposition times, Pt NPs are extremely small and possibly have higher energy band separation due to quantum confinement, preventing electron transfer from the TiO_2 conduction band (CB) to Pt.[12] But electrons can transfer freely to Pt NPs with an energy level lower than −4.4 eV (the lower energy level of the TiO_2 CB). As Pt NPs become larger, their properties may be approaching that of bulk Pt, capturing both photoelectrons and holes and acting as recombination centers.[12,24] Therefore, the optimal size of Pt NPs is that with energy bands positioned between −4.4 and −5.65 eV (work function of bulk Pt, see Figure 3 and Supporting Information, S8, for details). It should be noted that the particle number densities of the Pt NPs were kept constant (around 5×10^{12} no./cm^2) at various deposition times in this work (see Table 1), with least contribution to the decrease of charge carrier separation distance (CCSD), which is the reason for the increase of electron−hole recombination rates.[24] Thus it can be concluded that the Pt particle size plays an important role in the CO_2 photoreduction process. In this work, the optimal size was found to be around 1 nm, which is not readily achieved and controlled using liquid phase and other synthesis methods. Our methodology of angular RF sputtering method is promising and powerful. Although not exactly the same, gold NPs showed a similar size effect on the Fermi level equilibration of semiconductors, where smaller gold NPs can shift the Fermi level of TiO_2 to more negative potentials, resulting in enhanced photocatalytic performance.[25]

The CO_2 photoreduction mechanism of the Pt-TiO_2 nanostructured films is schematically shown in Figure 3. The extremely high photoreduction efficiency of the films is believed due to the synergistic effects of high surface area and minimized charge barriers by oriented single-phase crystallinity of the film and efficient electron−hole separation by the Pt NPs, as discussed above. Similar enhancement of CO_2 photoreduction efficiency was also achieved by Pt-TiO_2 nanotube arrays, where the Pt NPs were deposited on the TiO_2 nanotubes by using a rapid microwave-assisted solvothermal approach.[26]

The mechanism of CO_2 photoreduction is actually complex. Most researchers agree that this process is based on proton-assisted multielectron transfer (MET) instead of single electron transfer, as the electrochemical potential of −2.14 V vs SCE for a single electron process is highly unfavorable.[27] Depending on the number of electrons and protons, the formation products can be different. Carbon monoxide is formed by reacting with two protons and two electrons, while CH_4 formation needs

eight electrons and eight protons (see Supporting Information, S9, for details). The selective formation of CH_4 rather than CO is owing to the compromise between charge transfer and thermodynamics. The formation of CH_4 (E_{redox}/SCE = −0.48 V) is thermodynamically more feasible than the formation of CO (E_{redox}/SCE = −0.77 V) if the supply of protons and electrons is high enough.[27] Carbon monoxide was mainly obtained in many previous studies possibly due to the paucity of electrons. In this work, more electrons and protons were available. These electrons first reside on the Pt NPs and are then transferred rapidly from Pt to the absorbed CO_2 vapor for photoreduction (see Figure 3).[28] Our previous research revealed a similar phenomenon that Cu-doping could enhance the selectivity of CH_4 formation, as Cu species acting as electron traps resulted in an increased probability of multi-electron reactions.[6] Methane can also be formed by the depletion of CO following the six-electron reaction (Supporting Information, SE6) as seen in Figure 2b,[21] which also supports the selective formation of CH_4. Thermal effects are negligible in this work. The depletion of CO followed by oxidation with oxygen over the Pt surface is negligible in this work (see Supporting Information, S9), since the system was operated at atmospheric pressure and room temperature (Supporting Information, S10). Under these conditions, the chemisorption of both CO and O_2 on Pt surface is very weak, and the reaction rate is generally very slow.[29]

To further understand the charge carrier transfer dynamics, femtosecond time-resolved TA spectroscopy measurements were performed for both TiO_2 and Pt-TiO_2 samples with special focus on subnano- and nanosecond time range. Dependency of the electron−hole pair recombination rate constant (k_{obs}) on the pair concentration for both TiO_2 and Pt-TiO_2 films is shown in Figure 4. In both cases charge recombination rates are dependent on the excitation intensity (electron−hole pair concentration), and the observed trends can be fitted by linear functions. It is apparent that the linear fitting of the Pt-TiO_2 film has a gentler slope compared to its TiO_2 counterpart, indicating that the charge recombination process is slower for Pt-TiO_2. This is the direct evidence of Pt-driven suppression of the charge recombination process[30] in the Pt-TiO_2 sample, which is similar to that of Au-TiO_2.[25] Another evidence is that the linear fits converge to the same value of intrinsic electron−hole recombination rate constant ($k_{rec} \sim 0.22 \times 10^9$ s^{-1} or $\tau_{rec} \sim 4.5$ ns, Supporting Information, S11) if they are extrapolated to absorbance difference (ΔA) of zero. This is a hypothetical situation when charge recombination process is independent of electron−hole pair concentration and can be assumed as photogeneration of only one electron−hole pair per TiO_2 particle. The probability that a single electron is scavenged by Pt NPs instead of trapping in TiO_2 is very small, and therefore no difference should be observed between both samples.

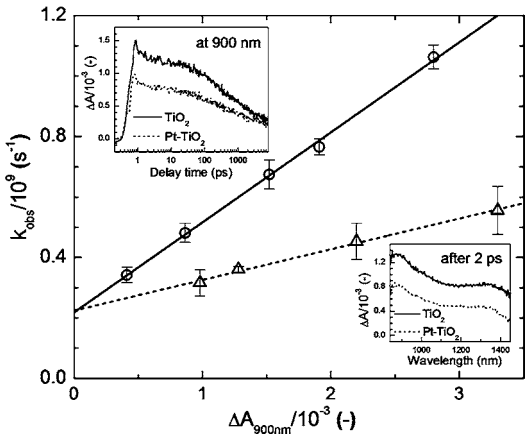

Figure 4. Time-resolved TA spectroscopy measurement results of TiO_2 and Pt-TiO_2 thin films (Pt deposition time of 45 s). The electron−hole pair recombination rate constant obtained from fitting of several TA kinetics of TiO_2 and Pt-TiO_2 films was recorded at 900 nm and plotted as a function of electron−hole pair concentration (expressed in ΔA). The lines represent linear fits. Solid line with open circles indicates TiO_2, and dashed line with open triangles is for Pt-TiO_2. Top-left inset: Representative TA kinetics of TiO_2 and Pt-TiO_2 films probed at 900 nm. Kinetics visibility was enhanced by expressing delay time in a logarithmic scale. Bottom-right inset: Representative TA spectra of TiO_2 and Pt-TiO_2 films taken in near-infrared spectral range. The spectra were recorded 2 ps after excitation.

■ CONCLUSIONS

In conclusion, we developed efficient Pt-TiO_2 nanostructured films using versatile gas-phase methods which can be produced at an industrial scale in an economically viable manner. The Pt-TiO_2 films in this work have demonstrated the highest photoreduction efficiency with selective formation of CH_4 reported to date, which is a high-quality fuel. While direct production of methane is preferred over CO (though a more toxic species) production is also fine as it is a constituent of syn gas and is used in the chemical industry to catalytically produce large number of products. The high surface area and single crystallinity of the unique 1D structure of the films and the efficient electron−hole separation by the Pt NPs were considered as the main reasons attributable for the enhancement. The low cost, scalable methodology illustrated for the design of functional photocatalysts with tailored morphologies can also be used for other reaction pathways and the synthesis of other catalytic materials.

■ ASSOCIATED CONTENT

Supporting Information

Extended details of methods used, additional characterization of Pt-TiO_2 films, photocatalytic pathways of CO_2 reduction, and time-resolved TA spectroscopy data set analysis. This material is available free of charge via the Internet at http://pubs.acs.org.

■ AUTHOR INFORMATION

Corresponding Author

pbiswas@wustl.edu

Author Contributions

#These authors contributed equally.

Notes

The authors declare no competing financial interest.

■ ACKNOWLEDGMENTS

This work was supported by the Consortium for Clean Coal Utilization (CCCU) at Washington University in St. Louis. Time-resolved spectroscopy measurements were carried out at the Photosynthetic Antenna Research Center (PARC), an Energy Frontier Research Center funded by the U.S. Department of Energy, Office of Science, Office of Basic Energy Sciences (DE-SC 0001035). Salary support for DMN was provided by PARC. Pt NP research was supported by the National Science Foundation (NSF GOALI-0523656). Partial

support from the Nano Research Facility (NRF, a member of NSF-NNIN) at Washington University in St. Louis is greatly acknowledged.

■ REFERENCES

(1) Metz, B.; Davidson, O.; de Coninck, H.; Loos, M.; Meyer, C. *IPCC Special Report on Carbon Dioxide Capture and Storage*; Intergovernmental Panel on Climate Change; World Meteorological Organization: Geneva, Switzerland, 2005.
(2) Usubharatana, P.; McMartin, D.; Veawab, A.; Tontiwachwuthikul, P. *Ind. Eng. Chem. Res.* **2006**, *45*, 2558.
(3) Indrakanti, V. P.; Kubicki, J. D.; Schobert, H. H. *Energy Environ. Sci.* **2009**, *2*, 745.
(4) Roy, S. C.; Varghese, O. K.; Paulose, M.; Grimes, C. A. *ACS Nano* **2010**, *4*, 1259.
(5) (a) Inoue, T.; Fujishima, A.; Konishi, S.; Honda, K. *Nature* **1979**, *277*, 637. (b) Iizuka, K.; Wato, T.; Miseki, Y.; Saito, K.; Kudo, A. *J. Am. Chem. Soc.* **2011**, *133*, 20863. (c) Takeda, H.; Koike, K.; Inoue, H.; Ishitani, O. *J. Am. Chem. Soc.* **2008**, *130*, 2023.
(6) Li, Y.; Wang, W. N.; Zhan, Z. L.; Woo, M. H.; Wu, C. Y.; Biswas, P. *Appl. Catal., B* **2010**, *100*, 386.
(7) Wang, W. N.; Park, J.; Biswas, P. *Catal. Sci. Technol.* **2011**, *1*, 593.
(8) Kraeutler, B.; Bard, A. J. *J. Am. Chem. Soc.* **1978**, *100*, 4317.
(9) Linsebigler, A. L.; Lu, G. Q.; Yates, J. T. *Chem. Rev.* **1995**, *95*, 735.
(10) Kim, S.; Choi, W. *J. Phys. Chem. B* **2002**, *106*, 13311.
(11) Bamwenda, G. R.; Tsubota, S.; Nakamura, T.; Haruta, M. *J. Photochem. Photobiol., A* **1995**, *89*, 177.
(12) Sadeghi, M.; Liu, W.; Zhang, T. G.; Stavropoulos, P.; Levy, B. *J. Phys. Chem.* **1996**, *100*, 19466.
(13) Lee, J. S.; Choi, W. Y. *J. Phys. Chem. B* **2005**, *109*, 7399.
(14) Woolerton, T. W.; Sheard, S.; Reisner, E.; Pierce, E.; Ragsdale, S. W.; Armstrong, F. A. *J. Am. Chem. Soc.* **2010**, *132*, 2132.
(15) An, W. J.; Thimsen, E.; Biswas, P. *J. Phys. Chem. Lett.* **2010**, *1*, 249.
(16) Yun, M. S.; Ramalingam, B.; Gangopadhyay, S. *Nanotechnology* **2011**, *22*, 465201.
(17) An, W.-J.; Jiang, D. D.; Matthews, J. R.; Borrelli, F.; Biswas, P. *J. Mater. Chem.* **2011**, *21*, 7913.
(18) Penn, R. L.; Banfield, J. F. *Science* **1998**, *281*, 969.
(19) Kim, B.; Byun, D.; Lee, J. K.; Park, D. *Jpn. J. Appl. Phys., Part 1* **2002**, *41*, 222.
(20) Lotgering, F. K. *J. Inorg. Nucl. Chem.* **1959**, *9*, 113.
(21) (a) Varghese, O. K.; Paulose, M.; LaTempa, T. J.; Grimes, C. A. *Nano Lett.* **2009**, *9*, 731. (b) Tanaka, K.; Miyahara, K.; Toyoshima, I. *J. Phys. Chem.* **1984**, *88*, 3504.
(22) Sasirekha, N.; Basha, S. J. S.; Shanthi, K. *Appl. Catal., B* **2006**, *62*, 169.
(23) Sahle-Demessie, E.; Gonzalez, M.; Wang, Z.-M.; Biswas, P. *Ind. Eng. Chem. Res.* **1999**, *38*, 3276.
(24) Gerischer, H. In *Photocatalytic Purification and Treatment of Water and Air*; Ollis, D. F., Al-Ekabi, H., Eds.; Elsevier Science Publishers B. V.: New York, 1993.
(25) Subramanian, V.; Wolf, E. E.; Kamat, P. V. *J. Am. Chem. Soc.* **2004**, *126*, 4943.
(26) Feng, X.; Sloppy, J. D.; LaTempa, T. J.; Paulose, N.; Komarneni, S.; Bao, N.; Grimes, C. A. *J. Mater. Chem.* **2011**, *21*, 13429.
(27) Morris, A. J.; Meyer, G. J.; Fujita, E. *Acc. Chem. Res.* **2009**, *42*, 1983.
(28) Wood, A.; Giersig, M.; Mulvaney, P. *J. Phys. Chem. B* **2001**, *105*, 8810.
(29) Su, X. C.; Cremer, P. S.; Shen, R. R.; Somorjai, G. A. *J. Am. Chem. Soc.* **1997**, *119*, 3994.
(30) (a) Furube, A.; Asahi, T.; Masuhara, H.; Yamashita, H.; Anpo, M. *Chem. Phys. Lett.* **2001**, *336*, 424. (b) Iwata, K.; Takaya, T.; Hamaguchi, H.; Yamakata, A.; Ishibashi, T. A.; Onishi, H.; Kuroda, H. *J. Phys. Chem. B* **2004**, *108*, 20233.